Order Parameters and Orientation Distributions of Solution Adsorbed and Microcontact Printed Cytochrome *c* Protein Films on Glass and ITO

Anne F. Runge,[†] Sergio B. Mendes,*,[†,‡] and S. Scott Saavedra*,[†]

Department of Chemistry and College of Optical Sciences, University of Arizona, Tucson, Arizona 85721

Received: October 21, 2005; In Final Form: January 13, 2006

The structure of solution adsorbed and microcontact printed (μCP) cytochrome *c* (cyt *c*) films on glass and indium tin oxide (ITO) was investigated using attenuated total reflectance (ATR) and total internal reflectance fluorescence (TIRF) spectroscopies to determine the orientation of the heme groups in the films. The second and fourth order parameters of the heme as well as information on the angle between the absorption and emission dipoles of the heme, γ, were experimentally determined. The order parameters of the heme are related to the order parameters of the protein molecule using the known angle between the heme plane and the electrostatic dipole moment of the cyt *c* protein. The effect of the surface roughness of the substrates (glass and ITO) was also taken into account quantitatively using AFM data. Physically possible order parameters were obtained for the heme group in both solution adsorbed and μCP films, but not for the electrostatic dipole moment of the protein. In addition, the experimental values of $\langle \cos^2 \gamma \rangle$ for immobilized zinc-substituted cyt *c* are greater than the values of $\langle \cos^2 \gamma \rangle$ determined in viscous solutions, which could be an indication that the environment of the heme groups changes upon adsorption. The electron transfer behavior of solution adsorbed and μCP films on ITO, determined using electrochemical methods, is compared to their orientation distribution and surface coverage as determined by spectroscopic methods.

1. Introduction

In many types of biosensors and bioassays, proteins have been used to modify the transducer surface for enhanced sensitivity and selectivity.[1–3] The surface of most proteins is heterogeneous, with areas of positive and negative charge, as well as hydrophobic regions. It remains a challenge to direct the adsorption and immobilization of such heterogeneous molecules onto artificial surfaces.[4,5] However, the structure and orientation of immobilized proteins can potentially have a large effect on their activity, and therefore on the sensitivity and selectivity of biosensors based on protein-modified surfaces. One example of this is the effect of surface immobilization on the electron transfer activity of metalloproteins.[6,7]

Cytochrome *c* (cyt *c*) is a widely studied redox active protein that undergoes stable electron transfer when immobilized on a variety of electrode surfaces.[8–12] The redox active component of the protein is a prosthetic heme group coordinating an iron-(III) which can be reduced to iron(II). The rate of electron transfer for surface immobilized cyt *c* can be varied by changing the distance between the electrode and the redox center of the protein. The most common electrode studied is gold, where the electrode–heme distance has been varied systematically using alkanethiol modifiers of different lengths.[13,14] Small changes in the distance (6–8 Å) can change the electron transfer rate by 3 orders of magnitude.[13,15] At long chain lengths (>10 carbons), the rate decreases exponentially with the number of methylene units, as predicted by Marcus theory.[14,15] At short chain lengths (<10 carbons), the rate is independent of chain length, which has been attributed to several factors, including conformational changes in the protein,[13] frictional coupling between the reactants and the surrounding environment,[14] and the increase in electric field strength close to the electrode surface.[15]

Changing the terminal group of the alkanethiol modifier can also change the electron transfer behavior and formal reduction potential of adsorbed cyt *c*.[16] This could be due to differences in the electronic coupling between the modifier and the protein or changes in the molecular orientation of the protein on the surface, or a combination thereof. Electrochemical data alone cannot distinguish between these two possibilities. Thus, while voltammetry can be a probe of how cyt *c* electrochemistry is affected by the terminal group of the self-assembled monolayer (SAM) film, the orientation distribution of the proteins cannot be inferred from electrochemical measurements alone.[8] In addition, since the electroactive surface coverage is usually not near the theoretical limit of one monolayer (22 pmol/cm² for cyt *c*),[17] it is possible that a significant portion of the adsorbed film is not contributing to the measured current.

The electrode used in this work is indium tin oxide (ITO), a semiconductor at which adsorbed cyt *c* can undergo stable, quasireversible electron transfer without a modifying layer.[18–21] ITO is negatively charged at pH 7, which has been hypothesized to direct oriented adsorption of cyt *c* through electrostatic interactions with basic residues on the surface of the protein. A similar mechanism is thought to direct cyt *c* adsorption to negatively charged SAMs on gold.[11] ITO is also transparent to visible light, making it a useful substrate for visible spectroscopy experiments.[22–24] We have studied cyt *c* electron transfer without modifying the electrode surface and attempted to change only the orientation distribution of the protein film. We are using two different deposition methods to attempt to create cyt *c* films with different orientation distributions. Solution adsorbed films

* To whom correspondence should be addressed. Voice: (520) 621-6340 (S.B.M.); (520) 621-9761 (S.S.S.). Fax: (520) 621-8407 (S.B.M.); (520) 621-8407 (S.S.S.). E-mail: sergiom@email.arizona.edu (S.B.M.); saavedra@u.arizona.edu (S.S.S.).
† Department of Chemistry.
‡ College of Optical Sciences.

Structure of Solution Adsorbed and μCP Cyt c Films

J. Phys. Chem. B, Vol. 110, No. 13, 2006 **6733**

are made by simply incubating the electrode in the protein solution, allowing the protein to directly adsorb. Microcontact printed (μCP) films are formed by first adsorbing the protein onto a poly(dimethylsiloxane) (PDMS) stamp and then transferring the protein film to a substrate by contacting it with the stamp. In recent years, microcontact printing has emerged as a technique that can be used to create patterned arrays of biomolecules for high throughput screening assays.[25-27] However, one aspect of this technique that has not been well characterized is the structure of the films formed by microcontact printing.[28-31] We have previously studied the electrochemical activity of μCP cyt c films on ITO and found they are similar in their electroactive surface coverage and formal reduction potential to solution adsorbed films.[32] However, the rate of electron transfer is slightly less than that of solution adsorbed films, which could be an indication of different orientation distributions. Characterizing the structure of μCP cyt c films on ITO can provide valuable information on the percentage of the film that retains its activity relative to the total amount of protein deposited on the electrode surface.

In the first paper of this series,[33] we have described the calculation of the second and fourth order parameters of molecular films using polarized attenuated total reflectance (ATR) and total internal reflectance fluorescence (TIRF) spectroscopies, as well as the use of the maximum entropy method, which can be used to construct orientation distributions from the order parameters. In addition, the treatment of the data described there allows for information on the angle between the absorption and emission dipoles, γ, to be determined from the TIRF data (using method B). Also described is a method to determine the influence of surface roughness on the second and fourth order parameters, and therefore the orientation distributions of the surface immobilized molecules. In this paper, order parameters are measured for four different types of cyt c films: (a) solution adsorbed films on glass and ITO and (b) μCP films on glass and ITO. The results show that the surface coverage and orientation distribution of cyt c films are dependent on the technique used to make the protein film and the substrate on which the protein film is formed. This work is one of relatively few papers that address molecular orientation distributions on electrode surfaces,[34,35] and it is the first to attempt to relate orientation distribution to electrochemical activity. Although a clear relationship between the orientation distribution and the electron transfer rate has not yet been elucidated, this work does illustrate the complexities of this subject and strategies for measuring and treating the data.

2. Combining ATR and TIRF Measurements for Cyt c

Two different types of cyt c are used in the data presented here. Ferricyt c is used in the ATR experiments to determine the second order parameter of the protein films. Zinc-substituted cytochrome c (Zn cyt c) is used as a fluorescent, nonelectroactive analogue of native cyt c in the TIRF measurements to determine the fourth order parameter. The vibronic transitions in the visible region of the spectrum of cyt c are polarized in the plane of the porphyrin. The heme group in cyt c has approximately D_{4h} symmetry,[36,37] which classifies the heme as a circular absorber,[38,39] although there is debate over the validity of this assumption.[40] The polarization ratio is the same at 413 and 530 nm,[39] an indication that a polarized absorbance measurement at any wavelength in this region will contain the same orientation parameter information. The absorbance of ferricyt films was measured at 413 nm, in the Söret band region, and used to determine $\langle \cos^2 \theta \rangle$, which is related to the second order
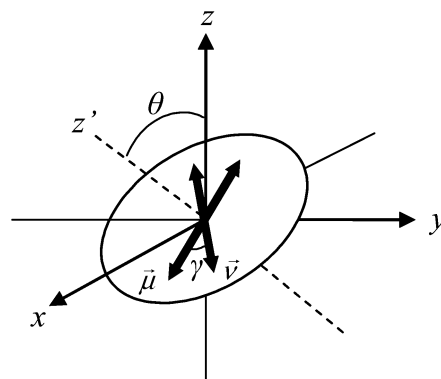

Figure 1. The molecular orientation of a circular absorber (heme) is defined by the x', y', and z' (only z' is shown) molecular axes which are related to the x, y, and z lab axes as shown. Both the absorption dipoles, $\vec{\mu}$, and the emission dipoles, $\vec{\nu}$, lie in the $x'-y'$ plane of the heme, and the angle between them is defined as γ. The angle between the axis normal to the heme plane and the lab surface normal is defined as θ.

parameter, $\langle P_2(\cos \theta) \rangle$.[33,41] As shown in Figure 1, θ is defined as the angle between the normal to the heme plane and the normal to the substrate surface (geometrically equivalent to the angle between the heme plane and the substrate surface). The TIRF experiment is used to determine $\langle \cos^4 \theta \rangle$, which is used along with $\langle \cos^2 \theta \rangle$ to calculate the fourth order parameter, $\langle P_4(\cos \theta) \rangle$. Here, films containing Zn cyt c were excited in the β-band at 585 nm. Our assumption is that even though we are probing two different transitions, they contain the same information about the orientation of the heme in cyt c.

3. Experimental Section

Protein Solutions. Horse heart cyt c (Sigma) was purified as previously described,[32,42] and its concentration was determined using published molar absorptivities.[43] Zn cyt c was prepared by first removing the iron from lyophilized cyt c (not purified) with hydrogen fluoride (HF) under anhydrous conditions.[44-46] Lyophilization was necessary to reduce side products of the HF reaction, which include heme-free cyt c (detected by MALDI). ***Safety Warning: HF gas is extremely dangerous, and all necessary safety precautions should be taken to avoid exposure.*** After HF treatment, the resulting iron-free cyt c was dissolved in a minimum amount of 50 mM pH 7 phosphate buffer and purified on a sephadex G-25 column equilibrated in the same buffer solution. Zinc acetate was reacted with the iron-free cyt c under acidic conditions,[37,47,48] and then the protein was dialyzed overnight against 35 mM pH 7 phosphate buffer. After centrifugation to remove any precipitate, the Zn cyt c was purified under the same conditions as ferricyt c. Fractions with an absorbance ratio of 423 nm/549 nm > 15.4 were collected and concentrated[47] in 10 mM phosphate buffer (pH 7) in an ultrafiltration cell. The final concentration was determined using the absorbance at 423 nm ($\epsilon = 243\ 000\ \text{M}^{-1}\ \text{cm}^{-1}$).[37]

Substrate Preparation. Glass microscope slides (Gold Seal) were cleaned either in a Chromerge (Manostat) bath at 60 °C for 1 h or in piranha solution (30% hydrogen peroxide, 70% concentrated sulfuric acid) for 1 h and rinsed thoroughly with deionized (18 MΩ cm) water before use. Indium tin oxide (ITO) films (65-70 nm thick) sputtered on 1 mm thick soda lime glass (Colorado Concept Coatings) with a sheet resistance of approximately 20 Ω per square were used throughout. The ITO substrates were cleaned by scrubbing them with a 2% Triton-X 100 solution for 1 min, then sonicating them for 10 min each

in 2% Triton-X 100, water, and ethanol,[49] and then low temperature air plasma cleaning (Harrick model PDC-3XG) for 15 min at 30 W. The PDMS stamps were made using a Sylgard-182 Elastomer kit (Dow Corning), mixing the monomer and curing agent in a 10:1 ratio. Flat (unpatterned) stamps were cured on oxidized Si wafers (Wacker) at 60 °C for 12–18 h. To prepare μCP films for TIRF experiments, circular PDMS stamps with a 1.0 cm diameter were punched out of the cured polymer film and mounted on metal stubs with epoxy. To prepare μCP films for ATR experiments, stamps of approximately 50 mm × 10 mm were cut from the cured polymer films and used to stamp one-half of the area of the ATR substrate.

Protein Films. Solution adsorbed films were made by injecting a 10 μM cyt c solution into the ATR flow cell or TIRF cell followed by a 15 min static incubation period and then rinsing the cell with 10 mL of 10 mM phosphate buffer. μCP films were formed using PDMS stamps that had been plasma treated to make their surfaces hydrophilic.[32] The stamp was rinsed with water and dried under a nitrogen stream before and after a 1 min air plasma treatment at 30 W (see above) and then soaked in a 160 μM cyt c solution for 15 min. The protein solution was then removed and the PDMS surface rinsed with three small aliquots of 10 mM phosphate buffer (pH 7). The stamp was then dried very slowly and gently under a nitrogen stream. Protein films were formed on ITO and glass by pressing the stamp onto the surface for less than 5 s, using light pressure sufficient to make conformal contact between the stamp and the surface. For ATR measurements, one-half the length of the glass or ITO substrate was printed with cyt c and then the printed side of the slide was soaked in 10 mM phosphate buffer and dried before placing the slide in the ATR cell. The volume of protein solution used to "ink" the stamp was approximately 0.5 mL, and the volume used to rinse the stamp was about 1.5 mL. For TIRF measurements, the volume of protein solution used to ink the stamp was approximately 0.15 mL and the volume used to rinse the stamps was approximately 0.5 mL (the volume decrease is due to the smaller stamp used in the TIRF measurements). For both solution adsorbed and μCP films, 100% ferricyt c was used to make the protein films for ATR measurements, while, for TIRF, protein films were composed of either 30% Zn cyt c and 70% ferricyt c or 10% Zn cyt c and 90% ferricyt c (mole percent). The fourth order parameter and $\langle\cos^2\gamma\rangle$ obtained from both types of films were equivalent; however, the signal-to-noise ratio improved for the 30% Zn cyt c films.

Attenuated Total Reflectance (ATR) Absorbance. The ATR instrument is described in a previous paper.[23,50] The absorbance of cyt c films in the transverse electric (TE) and transverse magnetic (TM) polarizations was measured through a 413 nm band-pass filter.[41] For solution adsorbed films, the blank transmission was measured before any protein was introduced to the surface. For μCP films, the ATR cell was translated on the y-axis (perpendicular to the direction of light propagation) to measure the blank transmission on the unprinted half of the slide before making the measurement on the printed half. This translation increased the error in the transmission measurement by 3% relative to the solution adsorbed films (in which the ATR cell was not moved during the course of the measurement).

Total Internal Reflection Fluorescence (TIRF). The inverted microscope and associated instruments used here for TIRF measurements are described in previous publications,[51,52] with the addition of a polarizer in the detection optics. The experimental setup will be briefly described here to highlight

changes. An argon ion laser (Coherent) was used in all-lines mode to pump a dye laser (Coherent 599) at 585 nm (rhodamine 6G). The excitation polarization was selected with a half-wave Fresnel rhomb. The laser excitation was coupled into the sample (mounted on the microscope stage) using a 45° angle prism (refractive index 1.46) coupled to the upper surface of the sample with index matching fluid. Fluorescence emission was collected with a 4× objective (0.13 NA) normal to the substrate surface and directed through a 635 ± 10 nm band-pass filter and a sheet polarizer onto a liquid nitrogen cooled CCD camera (Photometrics). The intensity of an unpolarized light source was measured after passing through the microscope optics, emission filter, and polarizer and reaching the CCD; no polarization bias was found. Each fluorescence image was background subtracted using an area in the same image, outside of the fluorescent spot, with the same pixel area as the fluorescent spot. To minimize the effect of photobleaching on the measurement, the four fluorescence intensities, $I_{s,s}$, $I_{s,p}$, $I_{p,p}$, and $I_{p,s}$,[33] were measured in a different order at each of four spots on a single sample. Different spots were selected by moving the sample perpendicular to the laser excitation (on the y-axis).[33] Then, an average for each of the four polarized fluorescence intensities was determined from the data of the four different spots. One value of $\langle\cos^4\theta\rangle$ was calculated per sample, and three independent samples were measured for each type of film. The laser power was measured after every set of four measurements, and it remained constant over the course of each sample measurement (within 2–5%).

AFM Images and Analysis. Glass and ITO surfaces were analyzed by tapping mode atomic force microscopy (Digital Instruments Multimode AFM) in air to determine the angle between the lab surface normal and the local surface normal, θ_3.[33] The $\cos^2\theta_3$ value for each data point in the AFM image (1 × 1 μm² area, 256 × 256 points, approximately 3.9 nm between points) was calculated using the method described by Simpson and Rowlen[53] to obtain the average two-dimensional local surface normal tilt angle and then averaged over the entire image to determine $\langle\cos^2\theta_3\rangle$. $\cos^4\theta$ was determined similarly for each point in the image and averaged over the entire image to calculate $\langle\cos^4\theta_3\rangle$. Three AFM images of each substrate were analyzed to determine the average values of $\langle\cos^2\theta_3\rangle$ and $\langle\cos^4\theta_3\rangle$.

4. Results and Discussion

This section is divided into five subsections. The first and second subsections report and discuss the data from the ATR and TIRF experiments. The third subsection discusses the order parameters and orientation distributions for the heme group. In the fourth subsection, the order parameters that describe the contribution of surface roughness and protein molecule orientation are reported and discussed. The final subsection discusses the orientation distribution and surface coverage of cyt c films formed on ITO in light of previous studies in which the electron transfer rate and electroactive surface coverage of the films was measured by cyclic voltammetry.[32]

Optical Constants, Surface Coverage, and $\langle\cos^2\theta\rangle$. The optical constants, surface coverage, and $\langle\cos^2\theta\rangle$ for solution adsorbed films on glass and ITO were reported in an earlier paper.[41] We summarize those results here and also report new data for μCP films on glass and ITO that were obtained in the manner described in the earlier paper (data for all four films are listed in Table 1). From the anisotropic optical constants n and k (the real and imaginary portions of the film complex refractive index, respectively), the surface coverage, Γ, and $\langle\cos^2\theta\rangle$ can be calculated.[41] The number of protein monolayers on

Structure of Solution Adsorbed and μCP Cyt c Films

J. Phys. Chem. B, Vol. 110, No. 13, 2006 **6735**

TABLE 1: Optical Constants, Surface Coverage, $\langle\cos^2\theta\rangle$, $\langle\cos^4\theta\rangle$, and $\langle\cos^2\gamma\rangle$ for Four Different Types of Cyt c Films Assuming the Heme Is a Circular Absorber

	method of deposition			
	solution adsorbed		μCP	
substrate	glass	ITO	glass	ITO
n_x, n_y (413 nm)	1.436 ± 0.008^a	1.53 ± 0.01^a	1.47 ± 0.03	1.515 ± 0.009
k_x, k_y (413 nm)	0.022 ± 0.002^a	0.045 ± 0.003^a	0.028 ± 0.005	0.050 ± 0.008
n_z (413 nm)	1.438 ± 0.009^a	1.52 ± 0.01^a	1.48 ± 0.03	1.485 ± 0.008
k_z (413 nm)	0.024 ± 0.003^a	0.042 ± 0.004^a	0.04 ± 0.01	0.017 ± 0.001
surface coverage (pmol/cm²)	11 ± 1^a	22 ± 1^a	22 ± 8	65 ± 10
$\langle\cos^2\theta\rangle$	0.30 ± 0.02^a	0.36 ± 0.04^a	0.19 ± 0.05	0.71 ± 0.01
% Zn cyt c	10 and 30	30	30	30
n_f (585 nm)	1.42	1.5	1.45	1.48
$\langle\cos^4\theta\rangle$	0.26 ± 0.04	0.19 ± 0.04	0.21 ± 0.04	0.66 ± 0.06
$\langle\cos^2\gamma\rangle$	0.86 ± 0.06	0.9 ± 0.3	0.84 ± 0.05	0.80 ± 0.03

[a] Error recalculated from results presented in an earlier paper[41] based on the standard deviation of three or five samples.

the surface can be estimated using the theoretical surface coverage of a close packed monolayer of cyt c, which is 22 pmol/cm² (based on the dimensions of cyt c).[17] This value assumes that the surface is flat; however, even when the ITO surface roughness is taken into account, the theoretical surface coverage per monolayer only increases to 23 pmol/cm² (calculated by analyzing AFM line scans of ITO surfaces to determine the ratio of the distance along the surface to the horizontal distance, which was 1.022).

In our previous report on solution adsorbed films, a thickness of 3 nm (based on the dimensions of cyt c[54]) was assumed for all of the films.[41] The surface coverage for μCP films was found to be more variable than solution adsorbed films and in many cases greater than one monolayer. Using a film thickness of 3 nm for these films would result in unreasonably high values for the optical constants n and k. Therefore, a change was made to the calculation procedure. For μCP films, the thickness was increased by increments of 3 nm until the surface coverage calculated per monolayer was less than or equal to 22 pmol/cm². For example, when 3 nm was used as the film thickness in the calculation, three out of five samples for μCP films on glass had surface coverage values that were less than one monolayer and remaining samples had calculated surface coverages greater than a monolayer. The calculations were repeated on these two samples using a thickness of 6 nm for the protein layer, and the resulting surface coverage per monolayer was less than 22 pmol/cm². For μCP films on ITO, a protein film thickness of 9 nm (three monolayers of protein) was used for two of the three samples, while a thickness of 12 nm was used for the third sample. The refractive index values for these films (Table 1) reflect a film where the density of protein is the same as that for a monolayer film, but the overall film thickness reflects a multilayer film.

We now compare the surface coverages of μCP films and solution adsorbed films (Table 1). The surface coverage of μCP films on glass is 22 ± 8 pmol/cm², and that on ITO is 65 ± 10 pmol/cm², which corresponds to about one and three monolayers of protein, respectively. The surface coverage of the solution adsorbed films were submonolayer (on glass) or monolayer (on ITO), with very little sample-to-sample variation. Thus, on both substrates, the surface coverage for the μCP films is greater than the solution adsorbed films. Furthermore, since the surface coverage was greater than or equal to one monolayer, then clearly more than one monolayer is adsorbed onto the PDMS stamp. This is most likely due to the high concentrations of protein used to ink the stamp (160 μM), which may favor more protein−protein interactions at the surface. High inking concentrations were used because they were shown in previous work

TABLE 2: Percent Relative Errors in Fluorescence Intensity Ratios

	soln ads glass	soln ads ITO	μCP glass	μCP ITO
$I_{s,p}/I_{s,s}$	8.5	47	5.3	7.7
$I_{p,s}/I_{p,p}$	4.0	11	0.8	9.0

to produce partially electroactive films on ITO.[32] The percent transferred from the stamp to the surface can vary depending on the surface chemistry and morphology of the substrate, which explains why the surface coverages for μCP films on glass and ITO differ. Furthermore, considerable variability is present in all of the steps of the μCP process (e.g., in the pressure applied to the stamp in contact with the substrate); thus, it is not surprising that the surface coverage of μCP films is more variable than that of solution adsorbed films.

Values of $\langle\cos^2\theta\rangle$ determined for all four films using the circular absorber model are listed in Table 1 (θ defined in Figure 1). All values are within the physically allowable range for $\langle\cos^2\theta\rangle$ (between 0 and 1).[33] The $\langle\cos^2\theta\rangle$ values for the μCP films are significantly different from each other and the solution adsorbed films, which both have similar $\langle\cos^2\theta\rangle$ values close to the isotropic value of $^1/_3$.

TIRF Results. Fluorescence intensities ($I_{s,s}$, $I_{s,p}$, $I_{p,p}$, $I_{p,s}$) were measured for the four types of films. Table 2 shows the percent error in the intensity ratios $I_{s,p}/I_{s,s}$ and $I_{p,s}/I_{p,p}$, as those ratios are independent of the intensity in the excitation laser beam. The errors on the ratios measured on ITO were generally higher than those on glass, most probably due to the higher fluorescence background of the ITO substrates.

$\langle\cos^4\theta\rangle$ values for the four types of films were calculated using method B (see preceding paper for details on method B) and reported in Table 1.[33] In addition to $I_{s,s}$, $I_{s,p}$, $I_{p,p}$, $I_{p,s}$, and $\langle\cos^2\theta\rangle$, the refractive indices of the protein film and the aqueous solution above the film as well as N, the effective index of the propagating optical beam (eq 3 in ref 41), must be known in order to determine $\langle\cos^4\theta\rangle$. The refractive index of the aqueous solution was obtained from literature values.[55] The refractive index of the protein films (n_x, n_y, and n_z at 413 nm) was calculated using the Kramers−Krönig transformations, as described in a previous paper.[41] In this case, it is assumed that there is no significant birefringence in the film, which is a reasonable approximation based on the ATR results that show $n_x \approx n_y \approx n_z$. The value of n_f at 585 nm was obtained by calculating the refractive index profile (from 400 to 700 nm) using the k values determined by ATR (at 413 nm) and the molar absorptivity values across the visible spectrum (values are reported in Table 1).[41] Figure 2 shows the molar absorptivity of ferricyt c and Zn cyt c as well as their refractive index profiles
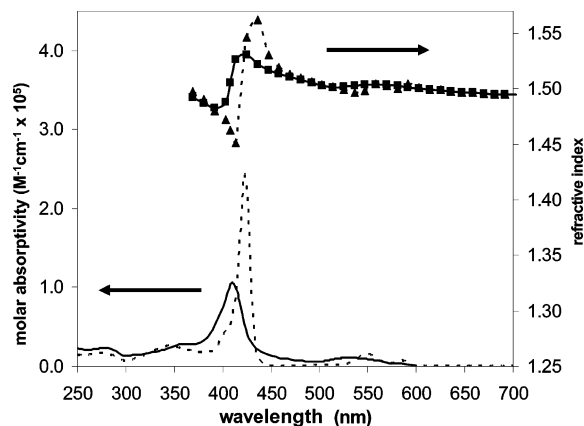
Figure 2. UV−visible absorbance spectra of ferricyt *c* (solid line) and Zn cyt *c* (dashed line) calculated using published molar absorptivity values.[43] Refractive index profiles for a concentration equal to one monolayer of each type of cyt *c* (0.73 M), calculated at discrete wavelengths for ferricyt *c* (solid line with squares at calculated points), and Zn cyt *c* (dashed line with triangles at calculated points).

for a full monolayer of protein. Despite the large differences in the molar absorptivities and refractive indices of ferricyt *c* and Zn cyt *c* in the Söret band region (400−450 nm), at 585 nm, at which Zn cyt *c* is excited in the TIRF experiments, the n_f values of ferricyt *c* and Zn cyt *c* are approximately equal.

Method B was used to calculate $\langle \cos^4 \theta \rangle$ and $\langle \cos^2 \gamma \rangle$ rather than method A because the use of the independently determined value of $\langle \cos^2 \gamma \rangle$ for Zn cyt *c* ($\langle \cos^2 \gamma \rangle = 0.5$; measured in viscous solution[17,34,56,57]) and method A produced values of $\langle \cos^4 \theta \rangle$ that were significantly greater than $\langle \cos^2 \theta \rangle$, which is outside the physically possible range of values (see preceding paper for details on method A[33]). The $\langle \cos^2 \gamma \rangle$ values of the films determined using method B are listed in Table 1 and range from 0.8 to 0.9. Assuming a delta function for γ, this range corresponds to angles between 27 and 18°. Values of $\langle \cos^2 \gamma \rangle$ greater than 0.5 indicate that the fluorescence emission dipole of immobilized Zn cyt *c* is not located with equal probability parallel or perpendicular to the absorption dipole in the heme plane. This could be an indication that the environment of the heme in Zn cyt *c* is altered upon adsorption to the surface. It is possible that immobilization of the protein on the surface distorts the structure of the protein such that the emission is no longer equally distributed between the two orthogonal dipoles but is more aligned with the absorption dipole. The fact that $\langle \cos^2 \gamma \rangle$ is not 0.5 does not rule out the circular absorber model because the two absorption dipoles could still be of equal strength; however, the fluorescence emission of immobilized Zn cyt *c* may not be generated equally along two orthogonal dipoles.[56]

The values of $\langle \cos^2 \gamma \rangle$ reported here represent the first direct measurement of $\langle \cos^2 \gamma \rangle$ for the porphyrin in an adsorbed heme protein film. The fact that $\langle \cos^2 \gamma \rangle$ can be calculated directly from measurements made on the film is an advantage of method B relative to method A, since the former can account for variations in γ arising from differences in the local environment of the chromophore.

Order Parameters and Orientation Distributions of the Heme Group. Using $\langle \cos^2 \theta \rangle$, second order parameters, $\langle P_2(\cos \theta) \rangle$, were calculated using eq 26 in the preceding paper.[33] Fourth order parameters, $\langle P_4(\cos \theta) \rangle$, were calculated from $\langle \cos^2 \theta \rangle$ and $\langle \cos^4 \theta \rangle$ using eq 27 from the preceding paper (see Table 3 for $\langle P_2(\cos \theta) \rangle$ and $\langle P_4(\cos \theta) \rangle$ values). In Figure 3a, the second and fourth order parameters for the solution adsorbed films and the μCP films on glass and ITO substrates are plotted. The area within the semicircle delineated by the solid line
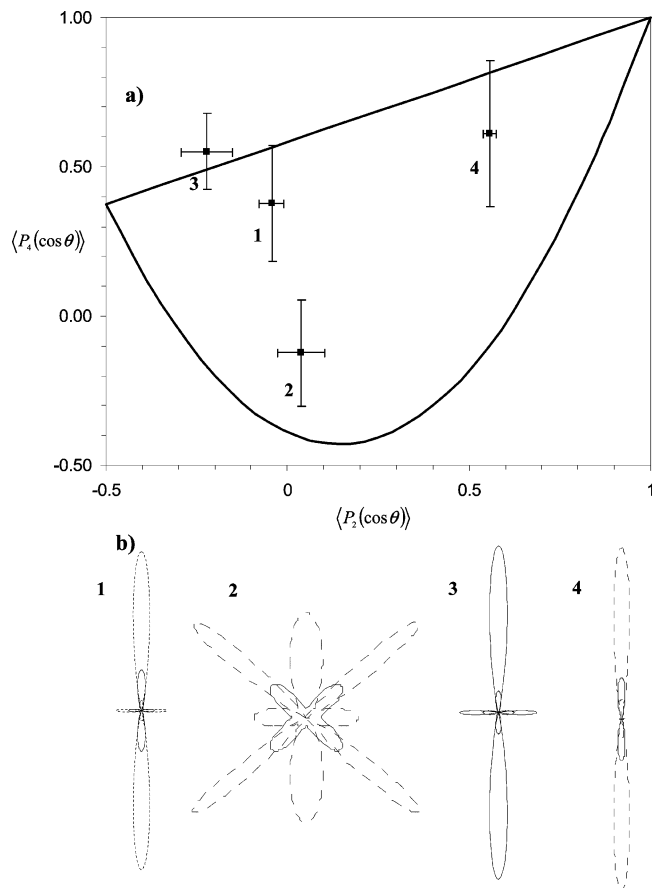

Figure 3. (a) Order parameters for the tilt angle of the axis normal to the heme and the lab normal (or the angle between the heme plane and the substrate plane) in cyt *c* films calculated using a circular absorber model for solution adsorbed films on glass (**1**) and ITO (**2**) and μCP films on glass (**3**) and ITO (**4**). The solid lines indicate the area of physically possible order parameters (see preceding paper[33]). (b) Polar plots of orientation distributions created from the corresponding order parameters. Solid lines represent the distributions created from the mean values of the order parameters. Dashed lines represent distributions created from values of order parameters that were one standard deviation from the mean values.

TABLE 3: Order Parameters for Cyt *c* Films Calculated Using a Circular Absorber Model

order parameter	soln ads glass	soln ads ITO	μCP glass	μCP ITO
$\langle P_2(\cos \theta) \rangle$	-0.04 ± 0.03	0.04 ± 0.07	-0.22 ± 0.07	0.56 ± 0.02
$\langle P_4(\cos \theta) \rangle$	0.4 ± 0.2	-0.1 ± 0.2	0.6 ± 0.1	0.6 ± 0.2
$\langle P_2(\cos \theta_3) \rangle$	0.99 ± 0.01	0.91 ± 0.06	0.99 ± 0.01	0.91 ± 0.06
$\langle P_4(\cos \theta_3) \rangle$	0.98 ± 0.02	0.7 ± 0.2	0.98 ± 0.02	0.7 ± 0.2
$\langle P_2(\cos \theta_2) \rangle$	0.8 ± 0.6	-0.8 ± 1	4 ± 1	-11.1 ± 0.9
$\langle P_4(\cos \theta_2) \rangle$	-1.1 ± 0.6	0.5 ± 0.7	-1.6 ± 0.4	-2 ± 1

represents the physically possible values of $\langle P_2(\cos \theta) \rangle$ and $\langle P_4(\cos \theta) \rangle$. The polar plots in Figure 3b show the orientation distributions that were calculated from the experimental $\langle P_2(\cos \theta) \rangle$ and $\langle P_4(\cos \theta) \rangle$ values using the maximum entropy method as described in the preceding paper[33] (also see ref 33 for an explanation of the polar plots). Orientation distributions were also constructed from values of the second and fourth order parameters one standard deviation away from the mean values.

On glass substrates, the orientation distribution constructed from the mean values of $\langle P_2(\cos \theta) \rangle$ and $\langle P_4(\cos \theta) \rangle$ for solution adsorbed films shows that the highest probability for the heme orientation is parallel to the substrate plane ($\theta = 0°$) (see Figure 3b, **1**). The orientation distribution of solution adsorbed cyt *c* films on glass has been studied in the past using a different

Structure of Solution Adsorbed and μCP Cyt *c* Films

J. Phys. Chem. B, Vol. 110, No. 13, 2006 **6737**

methodology, a different value of $\langle \cos^2 \gamma \rangle$ (0.57; determined in a viscous solution), and a Gaussian model for the distribution.[17] A different orientation distribution was obtained in which the mean tilt angle of the heme plane (the angle defined as β in that paper) relative to the substrate plane was 78° with a distribution width of 33°. The discrepancy between the results presented herein and those of Edmiston et al.[17] can be explained by examining the graph of allowed values of $\langle P_2(\cos \theta) \rangle$ and $\langle P_4(\cos \theta) \rangle$ and the resulting orientation distributions.[33] As shown in the preceding paper,[33] only the values near the lower boundary of allowed values can be fit by a Gaussian distribution. In the earlier study,[17] the experimentally determined order parameters did not fit a Gaussian distribution; therefore, values two and three standard deviations from the mean values were used to construct orientation distributions. Thus, the results presented herein do not contradict the previous study; rather, they clarify why the data obtained by Edmiston et al.[17] could not be fit with a Gaussian distribution.

For solution adsorbed films on ITO, the second and fourth order parameters are within one standard deviation of the isotropic values of zero (Figure 3a); therefore, the orientation distributions for these films are also very close to an isotropic distribution. This explains both the broadness of the distribution constructed from the mean values of the order parameters as well as the very different distributions constructed using order parameters differing by one standard deviation from the mean (Figure 3b, **2**). On the basis of these results, the orientation of the heme in cyt *c* solution adsorbed to ITO is close to random.

For μCP films on glass substrates, the mean values of $\langle P_2(\cos \theta) \rangle$ and $\langle P_4(\cos \theta) \rangle$ fall just outside of the range of allowed values (Figure 3a). Therefore, orientation distributions for these films were constructed using the mean value of the second order parameter and a value for the fourth order parameter that is one standard deviation less than the mean value. In the μCP films on both glass and ITO, the highest probability for the heme orientation is parallel to the surface, similar to the solution adsorbed films on glass (Figure 3b, **3** and **4**). These results suggest that the orientation distribution for μCP films is determined by the first step of the μCP printing process, in which protein is adsorbed to the PDMS stamp. This orientation distribution is then transferred to the substrate during the printing process. This hypothesis is supported by two pieces of data. First, the orientation distribution of the heme group in cyt *c* films on ITO differs depending on the method of formation. If the proteins in the μCP films reorient (rotationally diffuse) on the substrate surface after printing, the orientation distribution would be similar for both solution adsorbed and μCP films on ITO. The μCP printed films also have the same overall shape to their orientation distributions, regardless of the substrate to which they are transferred, while the solution adsorbed films have different orientation distributions depending on the substrate. Second, during the inking step, cyt *c* forms multilayers on the PDMS surface, and these are subsequently transferred intact to the substrate during printing (see Table 1 for surface coverage values). One possible explanation is that cyt *c* partially unfolds upon adsorption to PDMS, exposing hydrophobic residues, which cause the adsorption and denaturation of subsequent layers of protein.

Order Parameters of Cytochrome *c*. The following equation relates the order parameters of the heme in cyt *c* with order parameters that describe the protein molecule and the substrate:[33]

$$\langle P_{2n}(\cos \theta) \rangle = \langle P_{2n}(\cos \theta_3) \rangle \langle P_{2n}(\cos \theta_2) \rangle \langle P_{2n}(\cos \theta_1) \rangle \quad (1)$$

where *n* is either 1 or 2, denoting either the second or fourth order parameter, respectively. The order parameters $\langle P_{2n}(\cos \theta_1) \rangle$, $\langle P_{2n}(\cos \theta_2) \rangle$, $\langle P_{2n}(\cos \theta_3) \rangle$ are defined in the preceding paper.[33] Table 3 lists all of the second and fourth order parameters for the four types of cyt *c* films.

$\langle P_{2n}(\cos \theta_3) \rangle$ relates the lab (macroscopic) surface normal to the local surface normal, as they can be different due to microroughness on the substrate surface. Values of $\langle P_{2n}(\cos \theta_3) \rangle$ for glass and ITO surfaces were determined by analyzing tapping mode AFM images of these surfaces. $1 \times 1 \ \mu m^2$ AFM images were used so that the surface gradient[53,58] was calculated on a length scale (every 3.9 nm of the image) appropriate to the size of the cyt *c* molecule (projected surface area roughly 3×3 nm^2). If the substrate is perfectly flat, $\langle P_{2n}(\cos \theta_3) \rangle$ is 1 and this term drops out of eq 1. If the surface is very rough, $\langle P_{2n}(\cos \theta_3) \rangle$ approaches zero, and thus, $\langle P_{2n}(\cos \theta) \rangle$ will also approach zero. On glass, $\langle P_2(\cos \theta_3) \rangle$ and $\langle P_4(\cos \theta_3) \rangle$ are both nearly 1, indicating a relatively smooth surface (root mean square (rms) values of 0.1–0.4 nm). On ITO, $\langle P_2(\cos \theta_3) \rangle$ and $\langle P_4(\cos \theta_3) \rangle$ are 0.91 and 0.7, respectively, consistent with the fact that the surface of ITO (rms values between 1 and 2 nm) is much rougher than that of glass. Despite the increased roughness of ITO, $\langle P_2(\cos \theta_3) \rangle$ and $\langle P_4(\cos \theta_3) \rangle$ are not close to the isotropic value of zero, indicating that roughness of the substrate does not have a significant effect on the $\langle P_{2n}(\cos \theta) \rangle$ values.

$\langle P_{2n}(\cos \theta_1) \rangle$ is defined here as the relationship between the axis normal to the heme plane and the electrostatic dipole moment of the protein. The overall dipole moment of cyt *c* has been calculated from its crystal structure and is located at a 33° angle from the heme plane.[59] We chose this particular angle because it relates the heme (the spectroscopic probe) to the properties of the protein that control how the protein interacts with the surface (assuming that the dominant interaction is electrostatic[63]). Therefore, θ_1 is 57° and $\langle P_2(\cos \theta_1) \rangle$ and $\langle P_4(\cos \theta_1) \rangle$ are −0.055 and −0.352, respectively. Using $\theta_1 = 57°$ assumes that the position of the heme in the protein is unchanged after adsorption to glass or ITO. Since $\langle P_2(\cos \theta_1) \rangle$ is very close to the isotropic value of zero, the product of the order parameters in eq 1, $\langle P_2(\cos \theta) \rangle$, will also be close to zero, which complicates the analysis of protein orientation distribution (see below).

Using the assumptions stated above, eq 1 can be used to calculate $\langle P_2(\cos \theta_2) \rangle$ and $\langle P_4(\cos \theta_2) \rangle$ values, which are listed for the four types of cyt *c* films in Table 3. These order parameters describe the orientation of the adsorbed protein molecules on the basis of the electrostatic dipole moment of the protein relative to the local surface normal. In all four cases, the pairs of $\langle P_2(\cos \theta_2) \rangle$ and $\langle P_4(\cos \theta_2) \rangle$ values do not fall within the allowed range of physically possible values indicated by the solid lines in Figure 3. For solution adsorbed films, the standard deviations of $\langle P_2(\cos \theta_2) \rangle$ and $\langle P_4(\cos \theta_2) \rangle$ cover a wide range of values, including a range of physically possible pairs of values. However, there are many different orientation distributions within this range and thus a unique distribution cannot be specified.

There are at least two major factors that contribute to the recovery of pairs of $\langle P_2(\cos \theta_2) \rangle$ and $\langle P_4(\cos \theta_2) \rangle$ values that are not physically plausible: (a) It is possible that the defined orientation (33° angle) between the heme and the overall electrostatic dipole moment of the protein is not maintained upon surface adsorption; therefore, $\langle P_{2n}(\cos \theta_1) \rangle$ in eq 1 is not valid. (b) Even if the angle between the heme and the electrostatic dipole moment of the protein is maintained upon adsorption,

the value of $\langle P_2(\cos\theta_1)\rangle$ ($= -0.0551$) for cyt c is problematic because it is close to the isotropic value of zero. When $\langle P_2(\cos\theta_1)\rangle \approx 0$, the product of the order parameters on the right side of eq 1, $\langle P_2(\cos\theta)\rangle$, will also be ≈ 0. To solve eq 1 for $\langle P_2(\cos\theta_2)\rangle$, $\langle P_2(\cos\theta)\rangle$ (an experimental value close to zero with an error associated with it) must be divided by $\langle P_2(\cos\theta_1)\rangle$ (a very small number), which increases the uncertainty in $\langle P_2(\cos\theta_2)\rangle$. For example, the experimental values of $\langle P_2(\cos\theta)\rangle$ for the solution adsorbed films on glass and ITO are very close to zero and the calculated value of $\langle P_2(\cos\theta_2)\rangle$ for these films has a very large error associated with it (see Table 3).

Despite the fact that the analysis of cyt c films on glass and ITO presented here did not yield orientation distributions for the protein molecules based on their molecular dipole moment, this type of analysis is instructive and can be applied to other types of molecular films. The effect of such variables as surface roughness and the orientation of the chromophore relative to the molecule on any even numbered order parameter can be quantified using the methods described in the first paper of this series,[33] as illustrated experimentally here. It is clear from this analysis that the roughness of these substrates does not affect the order parameters of the film to any great extent. In future studies, a probe molecule with a $\langle P_{2n}(\cos\theta_1)\rangle$ value far from zero would be a better system to use for this type of analysis.

Correlation between Orientation Distribution, Surface Coverage, and Electron Transfer Behavior. Marcus theory predicts that the rate of electron transfer is dependent exponentially on the distance between the redox center of the protein and the electrode surface.[7,13,60] The heme in cyt c is positioned asymmetrically within the protein molecule.[54] Thus, in an adsorbed cyt c film, the heme-to-electrode distance distribution will be a function of the molecular orientation distribution. The issue addressed here is whether structural aspects of the cyt c films studied herein can be correlated with measurements of electron transfer rate and other electrochemical data. A number of factors must be considered. The most important is that the spectroscopic methods employed herein measure the properties of all protein molecules in the film, and cannot distinguish between adsorbed proteins that can be reversibly oxidized and reduced at the electrode surface versus those that are adsorbed but not electroactive. If the electroactive fraction of the film is <1, spectroscopic methods may not provide a representative picture of the structure of the electroactive fraction. The use of an ITO electrode may contribute to this discrepancy. The surface of ITO is very heterogeneous: a variety of functional groups are present,[49] and the surface conductivity varies on the micron length scale.[61] Thus, it is likely that some cyt c molecules adsorbed to ITO are electrochemically inactive because they are confined to regions of the electrode surface that are insulating.

In this discussion, we focus on solution adsorbed and μCP films on ITO, since it is clear from the spectroscopic results presented above that the structure of these films is considerably different, both in terms of surface coverage and heme tilt angle distribution. In a prior paper, we investigated differences in the electrochemical behavior of solution adsorbed and μCP films on ITO using cyclic voltammetry (CV).[32] The rates of electron transfer were determined to be 4.0 ± 0.5 and 3.0 ± 0.3 s^{-1}, respectively, and the difference between them was found to be statistically significant. The slower rate for μCP films suggests that the average distance between the heme group and the electrode surface is slightly greater (about 1 Å) in μCP films than in solution adsorbed films. The rate for both film types is consistent with a model in which the heme group is within 1

nm of the electrode surface.[60,62] The formal reduction potential and electroactive surface coverages of the films were also very similar. The issue that complicates further comparison between the CV data and the results presented here is that the electroactive (or electrochemical) surface coverage is much less than the total (spectroscopic) surface coverage. The solution adsorbed films are about 43% electroactive (22 pmol/cm^2 total surface coverage, 9.5 pmol/cm^2 electroactive), while the μCP films are about 12% electroactive (65 pmol/cm^2 total surface coverage, 8 pmol/cm^2 electroactive).[32] Thus, for solution adsorbed films, only half of the protein film is electroactive and contributes to the measured rate of electron transfer. For μCP films, only one-sixth of the film is electroactive. Therefore, the measured rates report on a subpopulation of the film, while the heme tilt angle distribution determined spectroscopically reports on the entire film. The electrochemical data do not contradict the heme tilt angles measured spectroscopically; however, a correlation between them cannot be established using the techniques reported here.

5. Conclusions

In summary, the second and fourth order parameters for four different types of cyt c films have been determined using ATR and TIRF spectroscopies. Experimental values for $\langle\cos^2\gamma\rangle$ were determined for surface immobilized Zn cyt c; they were consistent across the four types of cyt c films and differed from values of $\langle\cos^2\gamma\rangle$ determined in viscous solution. Orientation distributions for the tilt angle of the prosthetic heme group of the protein based on $\langle P_2(\cos\theta)\rangle$ and $\langle P_4(\cos\theta)\rangle$ were constructed using the maximum entropy method, modeling the protein as a circular absorber. The orientation distribution for solution adsorbed films on glass and μCP films on both glass and ITO show that the heme groups are oriented predominately parallel to the substrate plane. The orientation distribution of the heme groups in solution adsorbed films on ITO is very broad and nearly isotropic. The effect of the roughness of the substrate on the orientation distribution was found to be insignificant. It was not possible to reconstruct orientation distributions for the protein molecules relative to the local surface normal (θ_2) because the order parameters are not physically reasonable. One contributing factor might be the angle between the heme and the overall electrostatic dipole moment of the protein, assumed here to be 57°, which makes $\langle P_2(\cos\theta_1)\rangle$ almost isotropic and increases the uncertainty of the calculated value of $\langle P_2(\cos\theta_2)\rangle$. The work presented here also addresses relationships between the structure and the electroactivity of cyt c films on ITO; however, major differences in the total and electroactive surface coverages complicate this analysis.

References and Notes

(1) Gorton, L.; Lindgren, A.; Larsson, T.; Munteanu, F. D.; Ruzgas, T.; Gazaryan, I. *Anal. Chim. Acta* **1999**, *400*, 91.
(2) Wilner, I.; Katz, E. *Angew. Chem., Int. Ed.* **2000**, *39*, 1180.
(3) Zhang, W.; Li, G. *Anal. Sci.* **2004**, *20*, 603.
(4) Haynes, C. A.; Willem, N. *Colloid Surf., B* **1994**, *2*, 517.
(5) Zougrana, T.; Findenegg, G. H.; Willem, N. *J. Colloid Interface Sci.* **1997**, *190*, 437.
(6) Armstrong, F. A. *Struct. Bonding* **1990**, *72*, 137.

(7) Armstrong, F. A.; Heering, H. A.; Hirst, J. *Chem. Soc. Rev.* **1997**, *26*, 169.

(8) Kuznetsov, B. A.; Byzova, N. A.; Shumakovich, G. P. *J. Electroanal. Chem.* **1994**, *371*, 85.

(9) Reed, D. E.; Hawkridge, F. M. *Anal. Chem.* **1987**, *59*, 2334.

(10) *Cytochrome c: A Multidisciplinary Approach*; Scott, R. A., Mauk, A. G., Eds.; University Science Books: Sausalito, CA, 1996; p 738.

(11) Song, S.; Clark, R. A.; Bowden, E. F. *J. Phys. Chem.* **1993**, *97*, 6564.

(12) Wei, J.; Liu, H.; Dick, A. R.; Yamamoto, K.; He, Y.; Waldeck, D. H. *J. Am. Chem. Soc.* **2002**, *124*, 9591.

(13) Avila, A.; Gregory, B. W.; Niki, K.; Cotton, T. M. *J. Phys. Chem. B* **2000**, *104*, 2759.

(14) Khoshtariya, D. E.; Wei, J.; Liu, H.; Yue, H.; Waldeck, D. H. *J. Am. Chem. Soc.* **2003**, *125*, 7704.

(15) Murgida, D. H.; Hildebrandt, P. *J. Am. Chem. Soc.* **2001**, *123*, 4062.

(16) Chen, X.; Ferrigno, R.; Yang, J.; Whitesides, G. M. *Langmuir* **2002**, *18*, 7009.

(17) Edmiston, P. L.; Lee, J. E.; Cheng, S.; Saavedra, S. S. *J. Am. Chem. Soc.* **1997**, *119*, 560.

(18) Willet, J. L.; Bowden, E. F. *J. Electroanal. Chem.* **1987**, *221*, 265.

(19) Willet, J. L.; Bowden, E. F. *J. Phys. Chem.* **1990**, *94*, 8241.

(20) Daido, T.; Akaike, T. *J. Electroanal. Chem.* **1993**, *344*, 91.

(21) El Kasmi, A.; Leopold, M. C.; Galligan, R.; Robertson, R. T.; Saavedra, S. S.; El Kacemi, K.; Bowden, E. F. *Electrochem. Commun.* **2002**, *4*, 177.

(22) Bradshaw, J. T.; Mendes, S. B.; Armstrong, N. R.; Saavedra, S. S. *Anal. Chem.* **2003**, *75*, 1080.

(23) Doherty, W. J.; Donley, C. L.; Armstrong, N. R.; Saavedra, S. S. *Appl. Spectrosc.* **2002**, *56*, 920.

(24) Dunphy, D. R.; Mendes, S. B.; Saavedra, S. S.; Armstrong, N. A. *Anal. Chem.* **1997**, *69*, 3086.

(25) Epstein, J. R.; Biran, I.; Walt, D. R. *Anal. Chim. Acta* **2002**, *469*, 3.

(26) Kane, R. S.; Takayama, S.; Ostuni, E.; Ingber, D. E.; Whitesides, G. M. *Biomaterials* **1999**, *20*, 2363.

(27) Yang, S.; Perez-Luna, V. H.; Lopez, G. P. Two-Dimensional Patterning of Proteins. In *Protein Architecture*; Lvov, Y., Mohwald, H., Eds.; Marcel Dekker: New York, 2000; p 355.

(28) Graber, D. J.; Zieziulewicz, T. J.; Lawrence, D. A.; Shain, W.; Turner, J. N. *Langmuir* **2003**, *19*, 5431.

(29) Howell, S. W.; Inerowicz, H. D.; Regnier, F. E.; Reifenberger, R. *Langmuir* **2003**, *19*, 436.

(30) Inerowicz, H. D.; Howell, S.; Regnier, F. E.; Reifenberger, R. *Langmuir* **2002**, *18*, 5263.

(31) Patel, N.; Bhandari, R.; Shakesheff, K. M.; Cannizzaro, S. M.; Davies, M. C.; Langer, R.; Roberts, C. J.; Tendler, S. J. B.; Williams, P. M. *J. Biomater. Sci., Polym. Ed.* **2000**, *11*, 3199.

(32) Runge, A. F.; Saavedra, S. S. *Langmuir* **2003**, *19*, 9418.

(33) Runge, A. F.; Saavedra, S. S.; Mendes, S. B. *J. Phys. Chem. B* **2006**, *110*, 6721.

(34) Bos, M. A.; Kleijn, J. M. *Biophys. J.* **1995**, *68*, 2573.

(35) Yang, J.; Kleijn, J. M. *Biophys. J.* **1999**, *76*, 323.

(36) Sudha, B. P.; Dixit, N.; Waring, A. J.; Wells, K. O.; Wong, P. S.; Woodrow, G. V.; Vanderkooi, J. M. *Eur. J. Biochem.* **1982**, *126*, 1.

(37) Vanderkooi, J. M.; Adar, F.; Erecinska, M. *Eur. J. Biochem.* **1976**, *64*, 381.

(38) Ansari, A.; Jones, C. M.; Henry, E. R.; Hofrichter, J.; Eaton, W. A. *Biophys. J.* **1993**, *64*, 852.

(39) Eaton, W. A.; Hochstrasser, R. M. *J. Chem. Phys.* **1967**, *46*, 2533.

(40) Gryczynski, Z.; Paolesse, R.; Smith, K. M.; Bucci, E. *Biophys. Chem.* **1997**, *69*, 71.

(41) Runge, A. F.; Rasmussen, N. C.; Saavedra, S. S.; Mendes, S. B. *J. Phys. Chem. B* **2005**, *109*, 424.

(42) Brautigan, D. L.; Ferguson-Miller, S.; Margoliash, E. In *Methods in Enzymology*; Fleischer, S., Packer, L., Eds.; Academic Press: New York, 1978; Vols. 31,32, p 128.

(43) Margoliash, E.; Frohwirt, N. *Biochem. J.* **1959**, *71*, 570.

(44) Flatmark, T.; Robinson, A. B. Circular Dichroic Absorption Spectra of Cytochrome *c* from Bovine Heart and Cytochrome *c₂* from *Rhodospirilllum rubrum*. In *Structure and Function of Cytochromes*; Okunuki, K., Kamen, M. D., Sekuzu, I., Eds.; University Park Press: Baltimore, MD, 1968; p 318.

(45) Robinson, A. B.; Kamen, M. D. Some Observations on the Use of Hydrogen Fluoride in Cytochrome Degradation and Synthesis. In *Structure and Function of Cytochromes*; Okunuki, K., Kamen, M. D., Sekuzu, I., Eds.; University Park Press: Baltimore, MD, 1968; p 383.

(46) Vanderkooi, J. M.; Erecinska, M. *Eur. J. Biochem.* **1975**, *60*, 199.

(47) Tremain, S. M.; Kostic, N. M. *Inorg. Chim. Acta* **2000**, *300−302*, 733.

(48) Ye, S.; Shen, C.; Cotton, T. M.; Kostic, N. M. *J. Inorg. Biochem.* **1997**, *65*, 219.

(49) Donley, C.; Dunphy, D.; Paine, D.; Carter, C.; Nebesny, K.; Lee, P.; Alloway, D.; Armstrong, N. A. *Langmuir* **2002**, *18*, 450.

(50) The ATR instrument described in ref 23 was used here. However, the methodology described in ref 23 for determining the dichroism of the molecular film is incorrect and thus was not used here.

(51) Edmiston, P. L.; Lee, J. E.; Wood, L. L.; Saavedra, S. S. *J. Phys. Chem.* **1996**, *100*, 775.

(52) Phimphivong, S.; Kolchen, S.; Edmiston, P. L.; Saavedra, S. S. *Anal. Chim. Acta* **1995**, *307*, 403.

(53) Simpson, G. J.; Rowlen, K. L. *J. Phys. Chem. B* **1999**, *103*, 1525.

(54) Dickerson, R.; Kopna, M.; Weinzierl, J.; Warnun, J.; Eisenberg, D.; Margoliash, E. *J. Biol. Chem.* **1967**, *242*, 3015.

(55) Thormahlen, I.; Straub, J.; Grigull, U. *J. Phys. Chem. Ref. Data* **1985**, *14*, 933.

(56) Bos, M. A.; Kleijn, J. M. *Biophys. J.* **1995**, *68*, 2566.

(57) Tronin, A.; Edwards, A. M.; Wright, W. W.; Vanderkooi, J. M.; Blasie, J. K. *Biophys. J.* **2002**, *82*, 996.

(58) Simpson, G. J.; Rowlen, K. L. *J. Phys. Chem. B* **1999**, *103*, 3800.

(59) Koppenol, W. H.; Margoliash, E. *J. Biol. Chem.* **1982**, *257*, 4426.

(60) Bond, A. M. *Inorg. Chim. Acta* **1994**, *226*, 293.

(61) Liau, Y.; Scherer, N. F.; Rhodes, K. *J. Phys. Chem. B* **2001**, *105*, 3282.

(62) Gray, H. B.; Winkler, J. R. *Annu. Rev. Biochem.* **1996**, *65*, 537.

(63) The data published in ref 32 show that when adsorbed and *μ*CP cyt c films on ITO are rinsed in a high ionic strength buffer (10 mM phosphate plus 0.1 M NaCl), the electroactive surface coverage declines by approximately 50%. Protein desorption is the most probable cause for this decline and indicates that electrostatic interactions are a major contributor to the forces responsible for cyt c immobilization on ITO in lower ionic strength buffers (e.g., 10 mM phosphate).